Electronic Supplementary Material (ESI) for Lab on a Chip.

Electronic Supplementary Information

Mechanical-Activated Digital Microfluidics with Gradient Surface Wettability

Lin Qi[1#], Ye Niu[1,2#], Cody Ruck[1], and Yi Zhao[1*]

[1]Department of Biomedical Engineering, The Ohio State University, Columbus OH 43210

[2]Department of Mechanical and Aerospace Engineering, The Ohio State University, Columbus OH 43210

[#]: The authors contribute equally to this paper.

[*]: To whom all correspondence should be addressed: zhao.178@osu.edu

1. Energy Dissipation during Droplet Motion

There are two types of energy dissipation associated with the dynamics of a moving droplet [1-4]: viscous dissipation, and pinning/de-pinning of the contact lines. Viscous dissipation includes that near the rim of the contact lines and that in bulk. If the characteristic droplet size is greater than the critical capillary length:

$$\kappa^{-1} = \sqrt{\gamma/\rho g},$$

where γ is the surface tension of the liquid, ρ is the density, and g = 9.81 m/s^2 is the acceleration of gravity, the viscous dissipation is dominated by viscous dissipation in the bulk. Otherwise, the viscous dissipation is dominated by viscous dissipation near the rim of contact lines. For water at 25 ºC, κ^{-1} is 2.71 mm. For the largest droplet (60 μl) used in this work, the diameter or the maximal height of the droplet is 2.42 mm, which is less than κ^{-1}. Therefore, bulk viscous dissipation can be negligible. The droplet is mainly subject to the inertial force and the contact angle hysteresis induced adhesion force. To justify whether the dissipation associated with the contact line can be neglected, the energy inputs and losses during the droplet motion in the first half cycle, where the inertial force points towards the forward direction, are calculated.

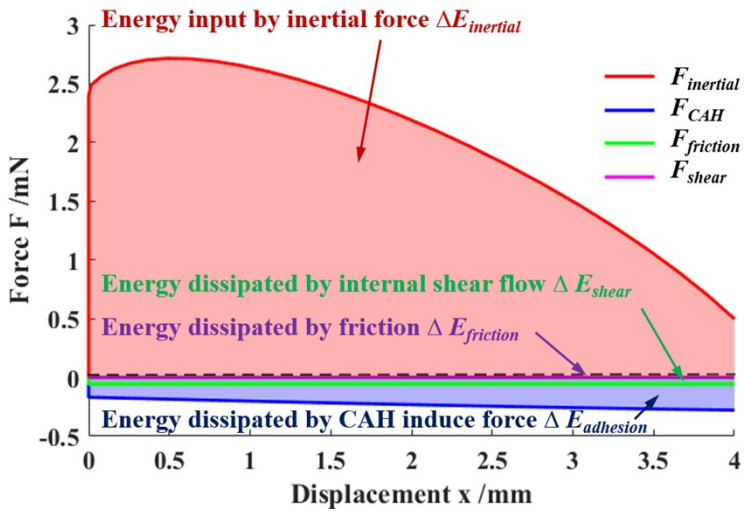

Figure S1. The relation of the forces and displacement during the motion of the droplet over one pattern length. The calculation is based on a 20 μL droplet moving on a pattern (4 mm × 2.5 mm) with wettability gradient from GS=10% ~ 18%. Driving frequency and amplitude are 9 Hz and 4 mm.

Specifically, the energy input and the energy dissipated during the half cycle when the droplet are moving towards the forward direction can be calculated as follows [5] and shown in **Figure S1**:

the work input by the inertial force:

$$\Delta E_{inertial} = \int_0^L F_{inertial} dx = \int_0^L mA_0(2\pi f)^2 sin2\pi ftdx \quad ;$$

the energy dissipated through the contact angle hysteresis induced adhesion force:

$$\Delta E_{adhesion} = \int_0^L F_{adhesion} dx = \int_0^L \gamma Cw(\cos\theta_r - cos\theta_a)dx \quad ;$$

the energy dissipated through the friction between the droplet and the substrate:

$$\Delta E_{friction} = \int_0^L F_{friction} dx = \int_0^L \eta mgdx \quad ;$$

the energy dissipated by the shear force induced by the internal flow structures of the droplet:

$$\Delta E_{shear} = \int_0^L F_{shear} dx = \int_0^L A_w \mu \frac{dV}{dy} dx$$; and

the energy dissipated through the deformation of the droplet:

$$\Delta E_{deformation} = \int_0^L \frac{V\gamma}{x} \left(\frac{D_{h1} - D_{h2}}{D_{h1} D_{h2}} \right) dx$$.

For a 20 μL droplet vibrating on a 4mm ×2.5mm pattern under the frequency of 9 Hz, the total energy loss is calculated as in **Table. S1**:

Table S1. The calculated energy inputs and energy losses during the first half of the vibration (based on a 20 μL droplet on a pattern (Length: 4mm × Width: 2.5mm) under the vibration frequency of 9 Hz and vibration amplitude of 4mm)

Notation	Value (J)
$\Delta E_{inertial}$	8.08×10^{-6}
$\Delta E_{adhesion}$	1.01×10^{-6}
$\Delta E_{friction}$	2.55×10^{-7}
ΔE_{shear}	1.86×10^{-9}
$\Delta E_{deformation}$	2.09×10^{-10}

As can be seen, the energy loss is mainly contributed by the contact angle hysteresis induced adhesion force which is considered in **Eqn.1** in the manuscript. Other sources of energy loss are significantly lower (at least one order of magnitude) than that induced by contact angle hysteresis. The total energy loss is only 15.4% of the energy input by the inertial effects of the vibration, mainly contributed by the contact hysteresis induced adhesion force. With higher vibration frequency, the ratio between the energy loss and energy input further decreases. Thus, it is plausible to neglect other energy loss without causing significance deviation. The experimental observations agreed well with the analytical model in the manuscript.

2. Surface Modification Mechanism

The change of surface hydrophobicity is due to the laser-induced change of both surface topography and surface chemistry.

The super-hydrophobic surfaces before and after laser treatments were examined. Scanning electron microscopy (SEM) images (Figure S2) showed that before treatment the super-hydrophobic coating contains both hierarchical topographies including both micro-bumps and nano-particles. After laser irradiation, surface roughness in the treated areas decreases as nanoparticles seem to aggregate and fuse.

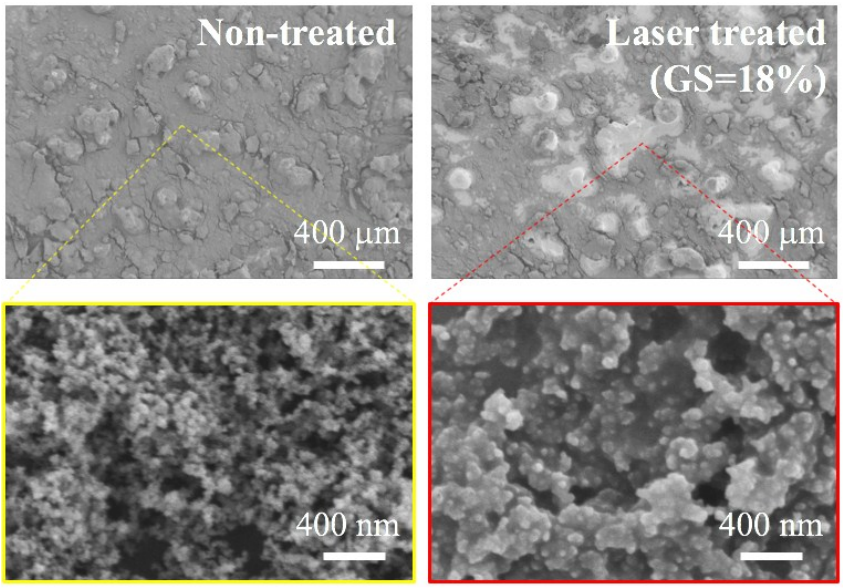

Figure S2: Topographical changes of the super-hydrophobic coating before and after laser treatment.

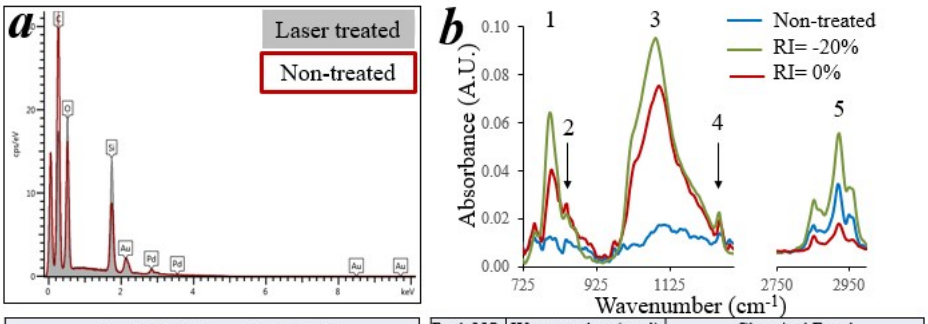

Atomic Ratio (normalized to Si)			
Element	Coating	RI=-20%	RI=0%
C	8.07	3.54	3.31
O	2.44	1.57	1.78
Si	1	1	1

Peak NO.	Wavenumber (cm^{-1})	Chemical Bond
1 ↓	789	$-CH_3$ rocking; Si-C stretching
2 ↑	825-865	Si-OH stretching
3 ↓	1050-1100	asymmetric Si-O-Si stretching
4 ↓	1257	symmetric $-CH_3$ deformation
5 ↓	2960	asymmetric Si-CH_3 stretching

Figure S3: Examination of surface composition. (a) EDS measurements; and (b) ATR-FTIR measurements.

The surface composition was examined by energy-dispersive X-ray spectroscopy (EDS) (**Figure S3a**). The measurement showed that the coating surface contains only C, O, and Si elements. Laser irradiation significantly decreases C/Si ratio, and modestly changes O/Si. The surface bonds were examined using attenuated total reflection-Fourier-transform infrared spectroscopy (ATR-FTIR) (**Figure S3b**). The measurements suggested that laser treatment reduces hydrophobic methyl groups ($-CH_3$), siloxane backbone (Si-O-Si) and increases polar groups (Si-OH), which both contribute to the decrease of surface hydrophobicity. This process is similar to laser-induced PDMS oxidation as we previous reported [6].

3. Hydrophobic Surface Reduces Surface Fouling

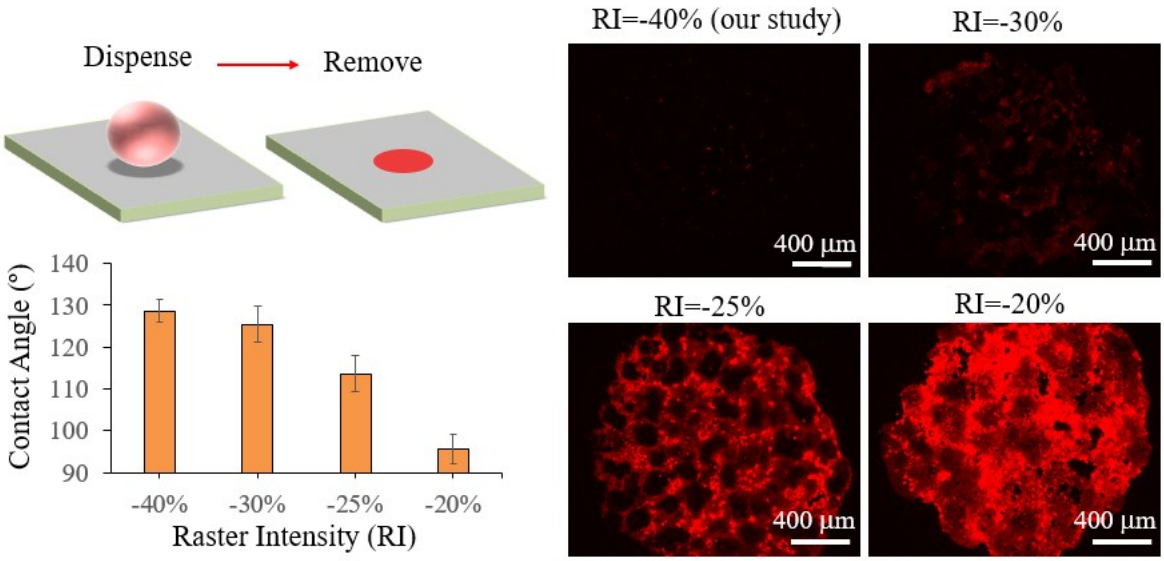

Figure S4: Examination of possible surface fouling using fluorescence labelled droplets. GS=18%, and the engraving cycles *n*=4 for all the samples.

4. Sustainability Test

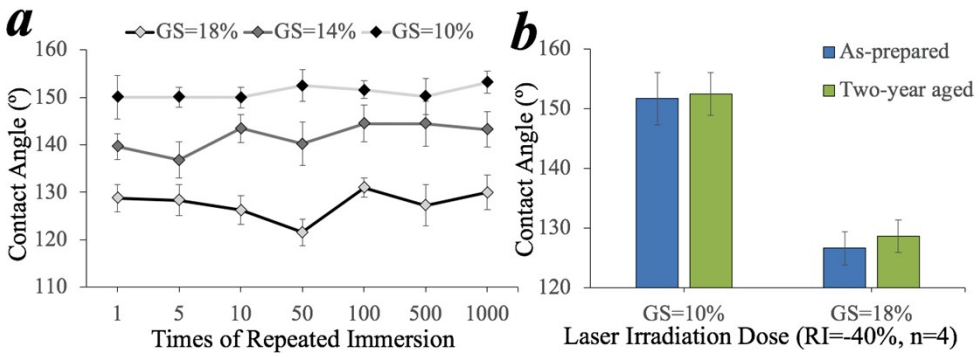

Figure S5: Sustainability of surface wettability: (a) by repeated immersion in water, and (b) by long time exposure in air.

5. Movie List

Movie 1: Side view of long-distance droplet translocation.

Movie 2: Top view of long-distance droplet translocation.

Movie 3: Droplet motion along a pre-determined two-dimensional trajectory.

Movie 4: Droplet motion under circular agitation.

Movie 5: Droplet mixing by moving two droplets toward opposite directions.

Movie 6: Selective manipulation of an array of droplets on the same substrate.

References:

1. Butt, H.J., et al., *Energy Dissipation of Moving Drops on Superhydrophobic and Superoleophobic Surfaces.* Langmuir, 2017. **33**(1): p. 107-116.
2. Chaudhury, M.K., A. Chakrabarti, and S. Daniel, *Generation of Motion of Drops with Interfacial Contact.* Langmuir, 2015. **31**(34): p. 9266-9281.
3. Chaudhury, M.K. and P.S. Goohpattader, *Activated drops: Self-excited oscillation, critical speeding and noisy transport.* European Physical Journal E, 2013. **36**(2): p. 15.
4. Chaudhury, M.K. and S. Mettu, *Brownian motion of a drop with hysteresis dissipation.* Langmuir, 2008. **24**(12): p. 6128-6132.
5. Yilbas, B.S., et al., *Water Droplet Dynamics on a Hydrophobic Surface in Relation to the Self-Cleaning of Environmental Dust.* Scientific Reports, 2018. **8**(1): p. 2984.
6. Qi, L., et al., *Writing Wrinkles on Poly (dimethylsiloxane)(PDMS) by Surface Oxidation with a CO2 Laser Engraver.* ACS applied materials & interfaces, 2018. **10**(4): p. 4295-4304.